Journal of King Saud University – Science 32 (2020) 2995–3004

Contents lists available at ScienceDirect

Journal of King Saud University – Science

journal homepage: www.sciencedirect.com

Original article

Theoretical modeling and experimental studies of Terebinth extracts as green corrosion inhibitor for iron in 3% NaCl medium

Mohammed Barbouchi [a,*], Bouchra Benzidia [b], Adnane Aouidate [c,d], Adib Ghaleb [e], Mostafa El Idrissi [a], M'barek Choukrad [a]

[a] Laboratory of Molecular Chemistry and Natural Substances, Department of Chemistry, Moulay Ismail University, Faculty of Science, B.P 11201 Zitoune, Meknes, Morocco
[b] Laboratory of Materials, Electrochemistry and Environment (LMEE), Department of Chemistry, Faculty of Science, Ibn Tofail University, BP 133, 14000 Kenitra, Morocco
[c] MCNSL, School of Sciences, Moulay Ismail University, B.P 11201 Zitoune, Meknes, Morocco
[d] CADD, Shenzhen Institute of Advanced Technology, Chinese Academy of Sciences, Shenzhen, China
[e] Laboratory of Analytical and Molecular Chemistry (LCAM), Department of Chemistry, Faculty Polydisciplinary Safi, Cadi Ayyad University, Safi 46030, Morocco

ARTICLE INFO

Article history:
Received 11 November 2019
Revised 1 August 2020
Accepted 7 August 2020
Available online 15 August 2020

Keywords:
Pistacia terebinthus
Corrosion inhibitor
Iron
3% NaCl
DFT
Molecular simulations

ABSTRACT

In this study, essential oils (EOs) obtained from twigs, leaves and fruits of Terebinth *(Pistacia terebinthus* L.) was characterized by GC/MS analysis. We tested these as green corrosion inhibitors for iron in the neutral chloride medium (3% NaCl), employing electrochemical impedance spectroscopy (EIS), potentiodynamic polarization (PDP) curves and surface characterizations SEM, EDX, IR spectroscopy were carried out. The theoretical aspect was elaborated using molecular dynamics (MD) simulation and density functional theory (DFT). Analyses of the experimental results showed that the three main components in the EOs from the twigs, fruits and leaves of Terebinth are α-Pinene (32.65–50.58%), Limonene (6.88–15.07%), and α-Terpineol (2.50–5.15%) with quantitative variations. The fruit EO at a concentration of 3000 ppm is characterized by the best anticorrosive protective properties than the leaf and twig EOs. Indeed, the optimum percentage of this EO required to achieve the maximum efficiency was found to be 86.4% at 3000 ppm. The surface investigation strategies (SEM-EDX and IR) further validated that the corrosion barrier happens because of the adsorption of the inhibitors over the iron/3% NaCl interface. Also, the outcomes of the theoretical approach supported all the experimental results by illustrating the similar trend of inhibition efficiencies of various inhibitors and revealed that Terebinth EOs could serve as an effective inhibitor of iron in 3% NaCl.

1. Introduction

Corrosion is a multifaceted phenomenon, defined as an interaction between metal or alloy and its environment resulting in deterioration of the main features of metals and their alloys (Chugh et al., 2020; Dehghani et al., 2019). The employ of inhibitors has been given to be one of the most popular and economic methods for the protection of metals or their alloys against corrosion in divers corrosive environments (Hamadi et al., 2018). The highly effective alternatives for the protection of metallic surfaces against corrosion are reached when using the green corrosion inhibitors (organic or inorganic). Although there is a great number of synthetic corrosion inhibitors that have proved an excellent corrosion inhibiting potential in the corrosive environments, a large part of them pose serious problems for human health, they are not cheap enough and raise major ecological issues (Dehghani et al., 2019; Haddadi et al., 2019). So, it is necessary to figure out alternative processes to find less expensive, readily available and non-toxic inhibitors. In the last decade, the considerable attention has been directed towards using plants as new sources for effective green corrosion inhibitors. Almost all natural organic compounds provide accessible, economical, safe and environmentally friendly alternative sources (Macedo et al., 2019; Sanaei et al., 2019). Usually, organic compounds owning heteroatoms such as nitrogen, sulfur or oxygen, electronegative groups, conjugated double bonds and aromatic rings exert significant effects on the extent of adsorption on the metal surface and they can therefore be applied securely as effective corrosion inhibitors (Qiang et al., 2018).

* Corresponding author.
E-mail address: med.barbouchi08@gmail.com (M. Barbouchi).

Peer review under responsibility of King Saud University.

Production and hosting by Elsevier

https://doi.org/10.1016/j.jksus.2020.08.004
1018-3647/

There are many fascinating reports about green corrosion inhibitors from various plant sources, which have been taken to mitigate the corrosion of metals or their alloys in the corrosive media. However, in the majority of these reports are concentrated to obtain a high inhibition efficiency but the economic aspect is almost ignored (Alibakhshi et al., 2019; Bahlakeh et al., 2019). We should also mention that certain of the green inhibitors derive from expensive sources or not completely available, as well as the use of organic solvents such as ethanol and methanol in the extraction procedure of the inhibitors from the whole plant or from any other part (twigs, leaves, fruits, seeds) makes the process expensive and also not eco-friendly (Bahlakeh et al., 2019; Majd et al., 2019). Furthermore, the process of extraction of the inhibitors based on water is most cost-effective in comparison with other polar solvents (like ethanol or methanol) and represents an advantage of ecological aspects (Dehghani et al., 2019; Haddadi et al., 2019).

It should be noted that the majority of current research on the significant inhibition of the innovative corrosion inhibitors (sustainable and green) derive from the plant-based was focused on corrosion control of metals or their alloys in acidic (sulfuric or hydrochloric) medium. Nevertheless, most of these eco-friendly inhibitors do not provide remarkable or impressive inhibition over neutral saline environment (Haddadi et al., 2019; Verma et al., 2018). Therefore, specific inhibitors of neutral saline media are needed, which go beyond what has so far been established to face threats from corrosion of metals. This leads us to look differently when choosing a green inhibitor for the appropriate application, several factors such as sustained availability of sources, extraction process (solvent), cost, best inhibition efficiency, and especially the environmental effects should be taken into account (Alibakhshi et al., 2019).

Over the past few years, researchers around the world reported most bioactive extracts derived from medicinal plants as promising green anticorrosive agents (Alvarez et al., 2018; Asadi et al., 2019; Barbouchi et al., 2019; Benzidia et al., 2019; Bozorg et al., 2014; Jokar et al., 2016). Even though a number of plants have been investigated in relation to their anticorrosive activity (Umoren et al., 2019; Verma et al., 2018), however, a large part of plants around the world have not been satisfactorily studied as anticorrosive agents. Therefore, there are considerable opportunities to discover out innovative, economical, novel, and eco-friendly corrosion inhibitors from this outstanding source of natural products.

Terebinth grows in dry areas, open woods and rocky, habitually calcareous slopes. It is native to the Canary Islands and the Mediterranean region from the western regions of Morocco, and Portugal to Greece and western Turkey (Rauf et al., 2017). It is therefore a species present and available in all around the Mediterranean. However, in this paper, the Terebinth EOs were extracted using hydro-distillation in Clevenger type apparatus. This means that it is really cost-effective and the extraction of inhibitor molecules from Terebinth would present so many environmental and economic benefits. In addition to that, it has been shown in literature that the EOs are biodegradable (Alparslan, 2018; Atarés and Chiralt, 2016). On the one hand, consumption of different organs (leaves, resin, flowers and fruits) from Terebinth is significantly higher over the Mediterranean countries and its history as a source of food traced back since antiquity (Foddai et al., 2015). Besides, all organs of Terebinth, including resin, leaves, gum, fruits, and twigs, have been used as valuable remedies for various kinds of diseases (Bozorgi et al., 2013; Rauf et al., 2017). All these main advantages, being low-cost, eco-friendly, biodegradable, available, harmless and readily obtainable have made Terebinth EOs an interesting corrosion inhibitors.

By considering all the above-mentioned factors, the present research is intended to use the Terebinth extracts for corrosion inhibition of iron in 3% NaCl solution. To our knowledge, this is the first time Terebinth EOs are applied as an environmentally friendly and cost-effective corrosion inhibitors source for iron in chloride media. In this case, the investigation seems to be interesting and relevant research, more than that it is a comparative study between the different parts of Terebinth in order to determine the most performant organs as a green corrosion inhibitor.

The main objective of this research is to study the influence of EOs extracted of twigs, leaves and fruits of Terebinth on the inhibition of corrosion from iron in chloride medium. The inhibition performance was provided via potentiodynamic polarization curves and electrochemical impedance spectroscopy; besides, surface studies were done by SEM/EDX. Furthermore, theoretical modeling was used to explore the adsorption of the molecules on the iron surface.

2. Material and methods

2.1. Plant material

Our *Pistacia terebinthus* L. plant were collected from Moulay Idriss Zerhoun a town in northern Morocco. The twigs, fruits and leaves of Terebinth were air-dried for 7 days at room temperature and the EO from each parts of Terebinth was obtained by hydrodistillation for 4 h and analyzes by GC/MS (Clarus SQ 8C Gas chromatograph coupled with mass spectrometer from PerkinElmer). We adopted the method describe in S1.

2.2. Electrochemical measurements

In this paper, the inhibitive action of EOs versus the iron corrosion in 3% NaCl solutions has been investigated. The composition of iron (wt%) employed in this research was as follows: Mn(0.514), Si (0.201), C(0.157), S(0.009), P(0.007), and Fe(balance).

The electrochemical measurements have been reached using a potentiostat/galvanostat in the SP-200. Three-electrode cell with an iron-working electrode of cylindrical shape (1 cm^2), a platinum electrode as counter-electrode, and reference electrode Ag/AgCl (XR300/XR310). Prior to use, the working electrode surface was washing with distilled water, shortly after successively abraded by SiC abrasive papers of grade 600 to 2000 on a rotating disc, followed by degreasing in ethanol and finally the samples are cleaned with distilled water. The working electrode is maintained prior to immersion in free corrosion potential during 30 min. The scanning speed is 1 mV/s.

The inhibition efficiency $\eta_{PDP}(\%)$ was estimated using the following relation Eq. (1) (Qiang et al., 2019):

$$\eta_{PDP}(\%) = \left[\frac{i^{\circ}_{corr} - i}{i^{\circ}_{corr}}\right] \times 100 \quad (1)$$

where i°_{corr} and i are corrosion current densities values without and with Terebinth EOs, respectively.

The plot of the EIS diagrams were conducted on a wave at frequency range between 100 KHz and 10 mHz and a potentiel amplitude of 10 mV on a steady state open-circuit potential (E_{ocp}). The inhibition efficiency $\eta_{EIS}(\%)$ was computed by the following formula Eq. (2) (Qiang et al., 2020):

$$\eta_{EIS}(\%) = \left[\frac{R_{p(inh)} - R_p}{R_{p(inh)}}\right] \times 100 \quad (2)$$

Were the $R_{p(inh)}$ and R_p represent the total resistance in the absence and presence of Terebinth EOs, respectively.

The PDP and EIS parameter fit was performed via EC-Lab software. In order to ensure reproducibility, all tests and measure-

ments are repeated three times. The evaluated inaccuracy did not exceed 10%.

2.3. Fourier transform infrared

Fourier transform infrared (FTIR) analysis was performed for Terebinth EO and for the formed film on the iron surface using FTIR spectrometer (type JASCO-4100) in order to illustrate the adsorbed functional groups. FTIR spectra were registered between 400 and 4000 cm^{-1}.

2.4. Surface analysis by SEM/EDX

The morphological characterization of the iron surface specimens was performed by SEM/EDX (scanning electron microscopy/the Energy Dispersive X-ray microanalysis), over the FEI Quanta 450 FEG.

2.5. Quantum chemical calculations

Computational science becomes an essential tool to determine compound inhibition, through a calculation of its interactions with the metal surface. Theoretical calculations were performed by Gaussian software version 09, using DFT/B3LYP and two different basis sets 6-311G** and 6-31G** in gas phase. Among the important global molecular properties that can describe chemical reactivity of organic compound as corrosion inhibitor are electronegativity (χ), chemical potential (μ), Global hardness (η), softness (S) and number of transferred electrons (ΔN):

The electronegativity (χ) and the hardness (η) are approximated as Eqs. (3) and (4) (Chugh et al., 2020):

$$\chi = \frac{I_P + E_A}{2} \tag{3}$$

and

$$\eta = \frac{I_P - E_A}{2} \tag{4}$$

where I_P is ionization potential ($-E_{LUMO}$) and $E_A$is electron affinity($-E_{HOMO}$).

The number of transferred electrons (ΔN_{110}) was defined as follows Eq. (5):

$$\Delta N_{110} = \frac{\varnothing - \chi_{inh}}{2(\eta_{Fe} + \eta_{inh})} \tag{5}$$

The function $\varnothing$ is the electronegativity of the metal surface, for Fe (110) surface it gives 4.82 eV (Haddadi et al., 2019). Also, the hardness of the iron surface (η_{Fe}) was predicted as 0.

The electrophilicity index (ω) is given by the following formula Eq. (6) (Domingo et al., 2016):

$$\omega = \frac{\mu^2}{2\eta} \tag{6}$$

Where the electronic chemical potential μ^2 = ((E_{LUMO} – E_{HOMO})/2).

The nucleophilicity index (N) has been recently introduced on the basis of the E_{HOMO} can be computed by the following expression Eq. (7) (Domingo and Pérez, 2011):

$$N = E_{HOMO}(Nucleophile) - E_{HOMO}(TCE) \tag{7}$$

The TCE (tetracyanoethylene) is taken as a reference owing to its lower E_{HOMO} in a large series of organic molecules.

The chemical softness (S) was introduced as the inverse of the chemical hardness Eq. (8) (Adib Ghaleb et al., 2018):

$$S = \frac{1}{2\eta} \tag{8}$$

The Fukui indices (FI) calculations were performed using the DMol3 module embedded in the Material Studio (MS, version 7.0) program of Accelrys Inc. They were calculated based on generalized gradient approximation (GGA) of Perdew–Burke Ernzerhof (PBE) and "double numeric plus polarization" (DNP, setting to 4.4) (Saha et al., 2014).

2.6. Molecular dynamics simulation

All studied compounds of EOs in this research were carried out via a simulation box along with periodic boundary conditions using materials studio package (Obot et al., 2015). As regards the iron crystal was imported, then cleaved alongside (1 1 0) plane and a slab of 5 Å was utilized. The surface of Fe (1 1 0) was relaxed by minimizing its energy employing the smart minimizer method. As well as the surface of Fe (1 1 0) was enlarged to a (10 × 10) supercell in order to envisage a wide surface for the interaction of studied inhibitors. Afterwards, a vacuum slab of 30 Å thickness was constructed overhead the Fe (1 1 0) plane. MD simulation were performed in a supercell with a size of a = b = 24,80 Å and c = 39,24 Å, containing 500 H_2O, 6 NaCl molecules and the tested inhibitors. As regards to simulation was achieved was made via a simulation box (24.82 × 24.82 × 35.69 $Å^3$) employing the forcite module with a time step of 1 fs and simulation time of 2000 ps carried out at 298 K, NVT ensemble, as well as COMPASS force field (Sun, 1998).

In simulation system, the interactions among Fe (1 1 0) and inhibitors were estimated using the following equations Eqs. (9) and (10) (Haddadi et al., 2019; Tan et al., 2020):

$$E_{interaction} = E_{tot} - \left(E_{Surface+solution} + E_{inhibitor}\right) \tag{9}$$

$$E_{Bindinig} = -E_{interaction} \tag{10}$$

where $E_{Surface+solution}$ assigned to the total energy of Fe (1 1 0) surface and solution without the inhibitors and $E_{inhibitor}$ present the total energy of inhibitors; E_{tot} indicate the total energy of the system as a whole.

3. Results and discussion

3.1. Chemical composition

The chemical composition found by GC/MS of EOs from twigs, leaves and fruits of Terebinth is presented in Table S2.

Forty-two and 36 compounds accounting for 98.74% and 98.48% of the EOs from twigs and leaves of Terebinth, as well as 45 compounds representing 99.53% of Terebinth fruit were characterized. In the Terebinth twig EO, the principal common constituents were α-Pinene (36.81%), Limonene (6.88%), β-Pinene (4.64%), α-Terpineol (3.97%), Undecan-2-one (3.70%) and β-Myrcene (3.50%). However, the leaf EO, α-Pinene (50.58%), Limonene (13.96%), Terpinolene (5.44%) and α-Terpineol (3.97%) were found to be the major components. Also, α-Pinene (32.65%), Limonene (15.07%), α-Terpineol (5.15%) and Terpinolene (5.44%) are the main constituents of fruit EO.

The three main components detected between the EOs from leaves, twigs and fruits of Terebinth are α-Pinene (32.65–50.58%), Limonene (6.88–15.07%) and α-Terpineol (2.50–5.15%) with quantitative variations.

3.2. Electrochemical methods

The objective of this section is to investigate the EOs from different organs of Terebinth in order to compare their inhibition efficiency against iron corrosion in 3% NaCl solutions. At first, we

started by investigating the Terebinth twig EO in order to find their optimal concentration. Afterwards, we'll be continuing our comparison study on the basis of this optimal concentration.

3.2.1. Electrochemical measurements of essential oil of Terebinth twig

Polarization curves and impedance diagrams of iron in 3% NaCl (free inhibitors) and containing various concentrations of Terebinth twig EO are illustrated in Fig. 1.

As shown in Fig. 1(a), there is a displacement of E_{corr} towards the anodic direction and the inhibition efficiency was found to increase with increasing of the inhibitor concentration from 1000 to 3000 ppm. The maximum inhibition efficiency was observed in the presence of 3000 ppm inhibitor. As regards the impedance curves (Fig. 1(b)), a presence of two loops is observed. The capacitive loop at high frequencies shows that the iron corrosion is mainly controlled by a charge transfer process. Furthermore, the inductive loop at low frequency values may be attributed to the relaxation process obtained by adsorption of EO inhibitors on the iron surface. However, the diameter of the capacitive loop in the presence of Terebinth twig EO is bigger than in the absence of EO inhibitors and increases with the EO concentration. The maximum value of the inhibition efficiency was evaluated at 71.6% for 3000 ppm.

Therefore, according to these results we'll be continuing our comparison study on the basis of this optimal concentration

3.2.2. Open circuit potential curves of different parts of Terebinth

The results of the open-circuit potential for iron in 3% NaCl without and with 3000 ppm of Terebinth EOs are reported in Fig. S3.

In the absence of the EOs inhibitors, the results show that the potential tends to stabilize at −0.52 V after 30 min. In the presence of EOs inhibitors, we note that the potential increases as soon as the leaf and fruit EOs is immersed, and then it stabilizes towards positive potentials. For the twig EO, the potential believes towards positive potentials as soon as our EO inhibitors is immersed. This change in potential indicates that the inhibitory effect acts preferentially on the anodic process.

3.2.3. Electrochemical measurements of different parts of Terebinth

- The polarization curves:

The polarization curves of iron in 3% NaCl, without and with the twig, leaf and fruit EOs of Terebinth, at 3000 ppm are presented in Fig. 2(a).

As it can be seen of Tafel polarization curves indicate that the adsorption of Terebinth EOs on the iron surface gives rise to a decrease in the current density compared to that of the blank (NaCl solution). This effect is ascribed to the modification of the reactional process owing the surface of the electrode is coated by a protective film, which accompanied with blocking of active sites. The film appears to inhibit effectively the anodic reaction at the corrosion potential and the same in its vicinity (Amar et al., 2007). We note there is a significant blocking of the anodic reaction proved by the shift of E_{corr} to the anodic direction. However, there is a limited effect on the cathodic reaction. The Tafel region of the cathodic portion that displays from −0.6 to 0.9 V/SCE this can be explained by the diffusion-controlled oxygen reduction reaction (Mehta et al., 2010). Usually, an inhibitor can be classified as the cathodic or anodic type when the change in E_{corr} value is above 85 mV with respect to that in the absence of the inhibitor (Aouniti et al., 2018). In the presence of EOs, E_{corr} shifts to more positive (about 82.43 mV) which indicates that the Terebinth EOs, can be classified as mixed-type inhibitors, with predominant anodic effectiveness. It is noted that when the potential reaches towards positive values of 300 mV, the anodic part is slightly modified. This result is well known as "desorption potential" and is coherent with other research that has found that an increase in anodic currents is primarily associated with the potential for desorption that varies significantly the inhibitor film (Bentiss et al., 2006). The results obtained in Table 1 suggest that the top inhibitor is the Terebinth fruit EO with an 88.7% efficiency.

- Impedance diagrams:

The corrosion behavior of iron in 3% NaCl solution in the absence and presence of EOs from various parts of Terebinth was investigated by the EIS method at room temperature after 30 min immersion. The results of this method are represented as Nyquist diagrams in Fig. 2 (b), and these capacitive loops are simulated by two equivalent circuits presented in Fig. 2(c) and (d). As an example, the Nyquist and Bode plots of both experimental and simulated data of iron in 3% NaCl solution without and with 3000 ppm of Terebinth EOs are exposed in Fig. 2 (c) and (d). In both circuits, R_S represent the resistance of the electrolyte, R_1 the resistance of the surface film, Q_1 is the capacitance due to the dielectric nature of the surface film. The R_2 is the charge transfer resistance related to the process corrosion with Q_2, which is an element of constant phase representing the ability of the double layer at the interface iron/3%NaCl solution. The impedance parameters acquired from these studies using EC-Lab software are displayed in Table 2.

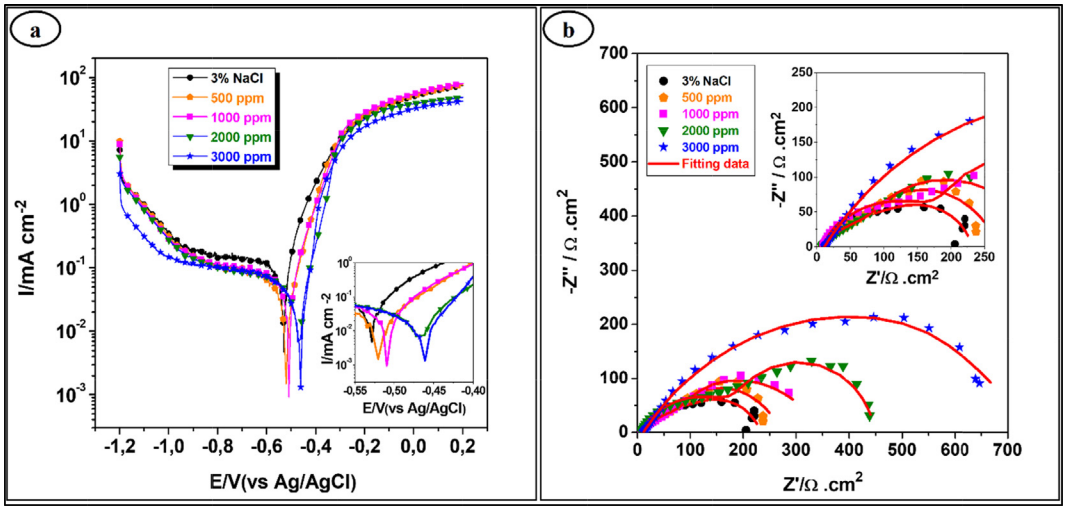

Fig. 1. (a) Polarization curves and (b) Nyquist plots for iron in 3% NaCl without and with different concentrations of Terebinth twig essential oil.

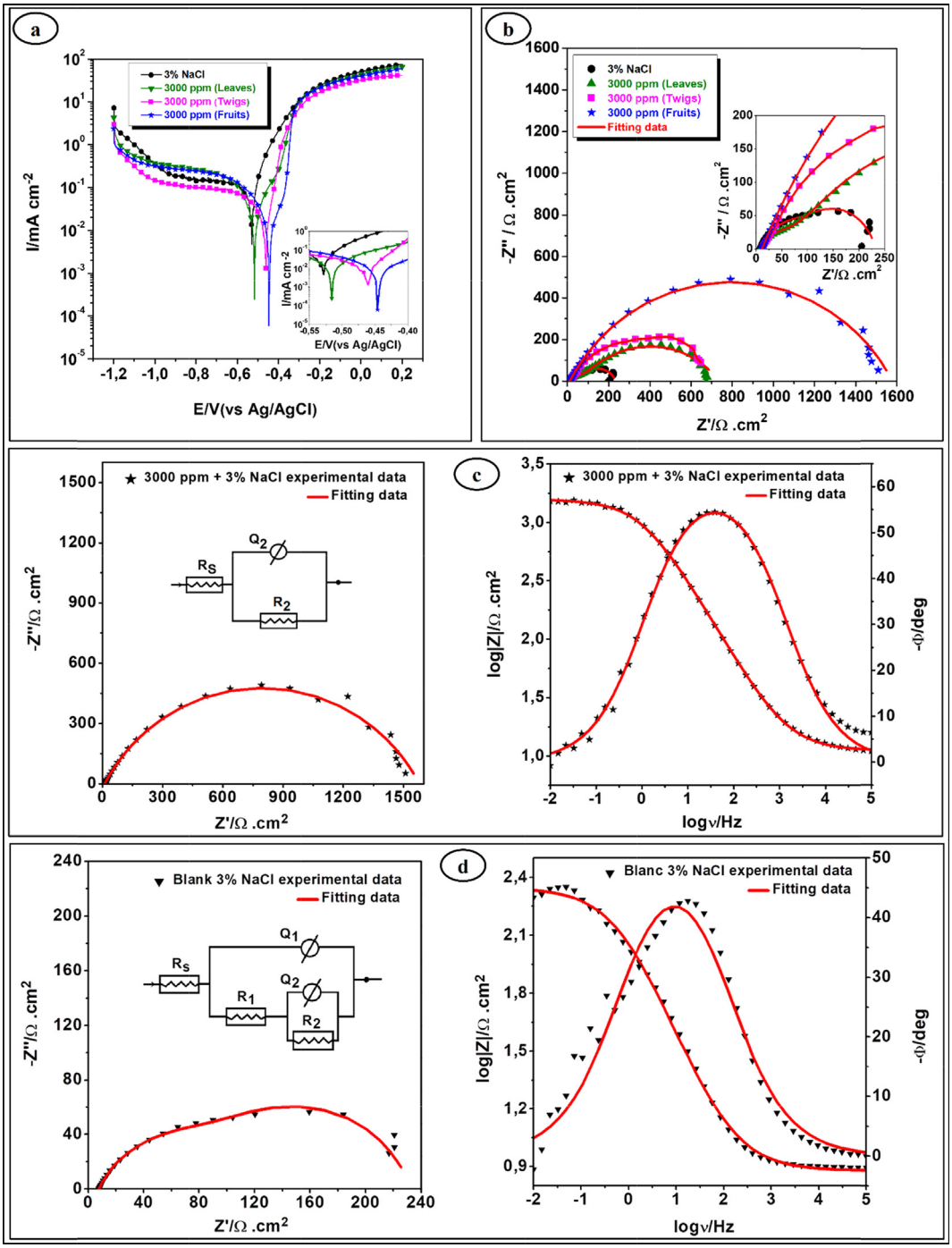

Fig. 2. (a) Polarization curves and (b) Nyquist plots for iron in 3% NaCl without and with 3000 ppm of Terebinth essential oils, EIS Nyquist and Bode plots for iron in 3% NaCl solution; (c) without, (d) with 3000 ppm of Terebinth fruit essential oil.

Table 1
Electrochemical parameters of the current-potential curves of iron in 3% NaCl.

		Concentration(ppm)	$-E_{corr}$(mV)	i_{corr}(μA/cm^2)	β_a(mV/dec)	-β_c (mV/dec)	η_{PDP}(%)
3% NaCl	Blank	———	527.51	78.23	76.5	464.4	———
Essential oils of Terebinth	Leaves	3000	517.1	29.2	125.8	138.7	62.7
	Twigs Fruits	3000	460.3	21.1	47.1	213.2	73.1
		3000	445.1	08.9	85.5	82.4	88.7

From Fig. 2a, the addition of inhibitors shows the appearance of two capacitive loops except in the case of the Terebinth fruit EO was the appearance of one loop, with an increase of the polarization resistance, this increase is more pronounced on the Terebinth fruit. In the high frequencies, the size of the capacitive loop increases than that in the blank solution, this can be allocated to

the formation of a protective film over the iron surface (Barbouchi et al., 2019). The low frequencies, the inhibitory effect results in an increase in the value of the charge transfer resistance R_2 that has a significant variation with inhibitors.

The inhibition efficiency value estimated from EIS data is in great agreement with those acquired from electrochemical polarization. However, in comparison with our previous results of the study of the EOs against iron corrosion in 3% NaCl solutions, it can say that the inhibition efficiency of the Terebinth fruit EO (86.4% at 3000 ppm) is better than that of *Pistacia lentiscus* (81.5% at 3000 ppm) (Barbouchi et al., 2019).

3.3. Immersion time effect

The evolution of the impedance diagrams, at different immersion times of iron in 3% NaCl, in the presence of 3000 ppm of the Terebinth fruit EO shown in Fig. 3. In this figure, it is observed that the electrochemical impedance diagrams for different immersion times in the presence of the Terebinth fruit EO (3000 ppm) look the same in size and shape with an increase in polarization resistance. These results show that the EO inhibitors does not degrade the protective film after 24 h, 48 h and 72 h immersion. These results reveal the protective effect of the Terebinth fruit EO and indicate that the thickness of the film seems to be enhanced by the immersion time.

3.4. Fourier transform infrared

Fig. S4 show the IR spectrum of the Terebinth fruit EO and the corrosion product on the iron surface in the presence of inhibitors. The spectrum S4(a) of the Terebinth fruit EO shows a large peak at 3422.45 cm^{-1}, which could be assigned to O-H stretching mode. The bands appearing at 2921.37 and 2845 cm^{-1} corresponded to C–H stretching vibrations. The peak at 1730.52 cm^{-1} corresponded to the C=O stretching vibrations. The C=C stretching vibration was detected at 1637.25 cm^{-1}. The peak at 1403 cm^{-1} could be due to binding C–H in plan and the bands appearing at 882.78 and 787.62 cm^{-1} corresponded to the aromatic ring. On comparing Fig. S4(a) and (b) shows that the certain additional peaks have appeared and few have shifted to higher frequency region, providing that some interaction/adsorption has been taking place over the metal surface. The –OH stretching shifted from 3422.45 to 3434.22 cm^{-1} and C=O stretching shifted from 1730.52 to 1741.16 cm^{-1} may be confirmed that there is a strong interaction between EO inhibitors and the iron surface.

3.5. Surface analysis

SEM/EDX techniques were carried out to establish the interaction of EOs inhibitors with the metal surface after immersion for 24 h in 3% NaCl solution. Fig. 4(a_1) shows a plan view of SEM micrograph of the blank (without inhibitors) sample, which is clearly corroded and characterized by a highly rough surface with corrosion products on the surface. In the presence of inhibitors Fig. 4(b_1, c_1 and d_1), iron surface damage was strongly reduced and the coupons appeared smooth. This observation supported

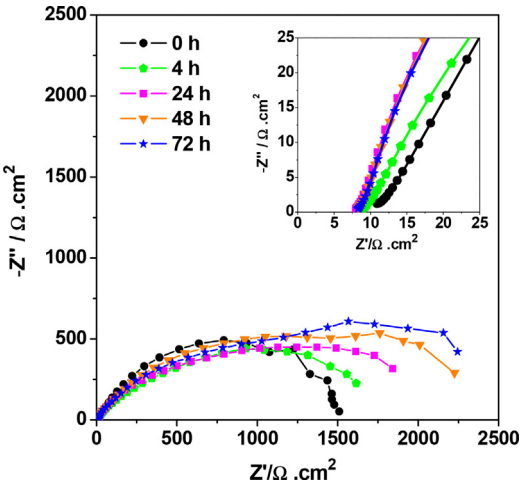

Fig. 3. Nyquist plots of the sample immersed in 3% NaCl solutions as a function of time, including 3000 ppm of Terebinth fruit essential oil.

the formation of a protective barrier layer on the iron surface after 24 h exposure to the corrosive media containing 3000 ppm of Terebinth EOs. EDX was employed to determine the elements present on the iron surface without and with Terebinth EOs. Fig. 4(a_2) illustrates that in the absence of the EOs inhibitors (blank), the spectra contained mainly the characteristic peaks of Fe, C, O, Cl and Na. This suggested the formation of metal oxides/hydroxides and chlorides as corrosion products on the iron surface. In the presence of the EOs inhibitors Fig. 4(b_2, c_2 and d_2), we remarked the reduction in peak intensity of O also makes the Cl and Na disappear. Hence, we could say that the molecules of Terebinth EOs adsorbed on the iron surface, preventing the formation of oxides/hydroxides and chlorides. In addition, the percentage of carbon increases because it is related to the chemical composition of our inhibitors indicating the adsorption of the EOs inhibitors on the iron surface leading to the creation of a protective film.

3.6. Theoretical calculation

- Quantum chemical calculations

DFT was employed to explore the atomic sites having an impact on the adsorption of α-Pinene, Limonene, α-Terpineol, p-Cymen-8-ol and p-Cymene on the metallic surface using two different basis sets 6-311G** and 6-31G** to determine and confirm the reliability of calculations results. The choice of these molecules is based on the fact that α-Pinene, Limonene and α-Terpineol are the main components detected between the EOs from leaves, twigs and fruits of Terebinth. On the other hand, the p-Cymen-8-ol and p-Cymene are chosen because they own the electron-rich centers. The global indices; μ, η, ω, N and ΔN were calculated and dipected in Table 3.

The tendency of the inhibitors (molecules) to donate electrons can be acknowledged by the high values of N are classified as strong nucleophile, whereas further insights of capacity to accept

Table 2
The electrochemical parameters derived from impedance diagrams.

	C 3000 ppm	R_s (Ω.cm^2)	R_1 (Ω. cm^2)	$Q_1 \times 10^{-3}$ F s$^{(n-1)}$	n_1	R_2 (Ω. cm^2)	$Q_2 \times 10^{-3}$ F s$^{(n-1)}$	n_2	R_p (Ω. cm^2)	η_{EIS}(%)
3% NaCl	Blank	7.8	87.6	1.11	0.73	128.6	6.57	0.93	216.1	–
Essential oils of Terebinth	Leaves	8.9	77.9	0.24	0.69	649.9	0.36	0.58	727.8	70.3
	Twigs	11.1	160.7	0.72	0.63	601.4	0.21	0.66	762.1	71.6
	Fruits	11.1	–	–	–	1587	0.17	0.69	1587	86.4

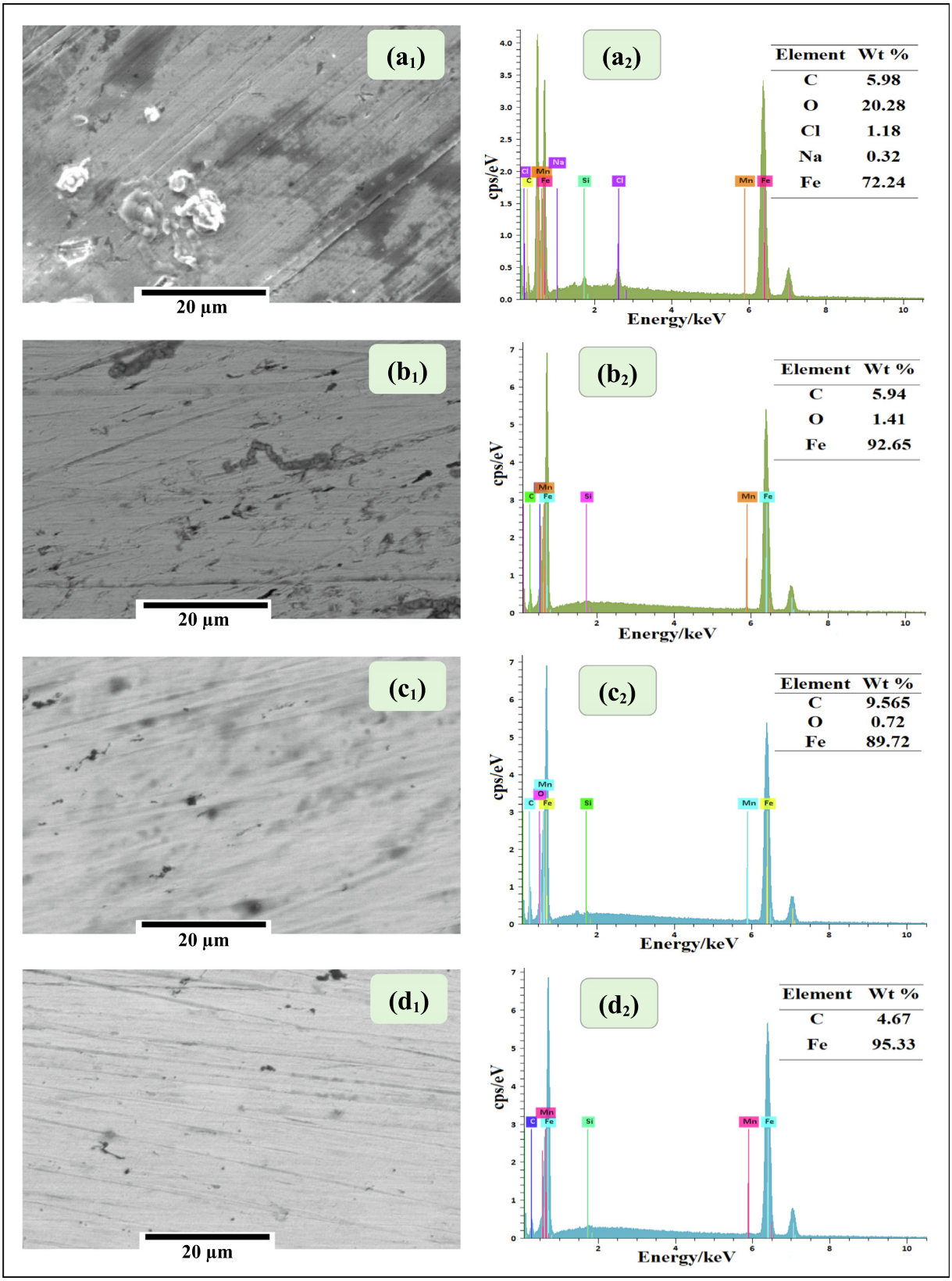

Fig. 4. SEM/EDX analysis of the iron dipped in the 3% NaCl solution without ((a_1, a_2) blank) and with 3000 ppm of essential oils from (b_1, b_2) leaves, (c_1, c_2) twigs, and (d_1, d_2) fruits of Terebinth.

electrons is indicated by the high value of ω are classified as strong electrophile (El Aoufir et al., 2016). Therefore, the ΔN value donates a measure of the capacity of a chemical compound to transfer its electrons to the metal if $\Delta N > 0$ and vice versa if $\Delta N < 0$ (Kovačević and Kokalj, 2011). The positive values of ΔN displayed in Table 3, illustrates that the high ability of studied inhibi-

Table 3
The energies of *HOMO/LUMO*, ionization potential (I_P), electron affinity (E_A), electronegativity (χ), hardness (η), electrophilicity (ω) nucleophilicity (N), softness (S), and the fraction of electrons transferred (ΔN) for compounds inhibitors using B3LYP/6-31G**; 6-311G**.

Inhibitors	E_{HOMO} (eV)	E_{LUMO} (eV)	I_p	E_A	χ	η	ω	N	S	ΔN
B3LYP/6-311G**										
α-Pinene	−6.072	0.374	6.072	−0.374	2.849	3.223	1.259	3.28	0.155	0.306
Limonene	−6.303	0.244	6.303	−0.244	3.030	3.273	1.402	3.06	0.153	0.273
α-Terpineol	−6.303	0.439	6.303	−0.439	2.932	3.371	1.275	3.06	0.148	0.280
p-Cymene	−6.394	0.176	6.394	−0.176	3.109	3.285	1.472	2.96	0.152	0.260
p-Cymen-8-ol	−6.328	−0.190	6.328	0.190	3.259	3.069	1.730	3.03	0.163	0.254
B3LYP/6-31G**										
α-Pinene	−5.852	0.703	5.852	−0.703	2.574	3.278	1.011	3.50	0.153	0.343
Limonene	−6.084	0.608	6.084	−0.608	2.738	3.346	1.120	3.27	0.149	0.311
α-Terpineol	−6.083	0.840	6.083	−0.840	2.621	3.462	0.992	3.27	0.144	0.318
p-Cymene	−6.164	0.174	6.164	−0.174	2.995	3.169	1.415	3.19	0.158	0.288
p-Cymen-8-ol	−6.094	0.154	6.094	−0.154	2.970	3.124	1.412	3.26	0.160	0.296

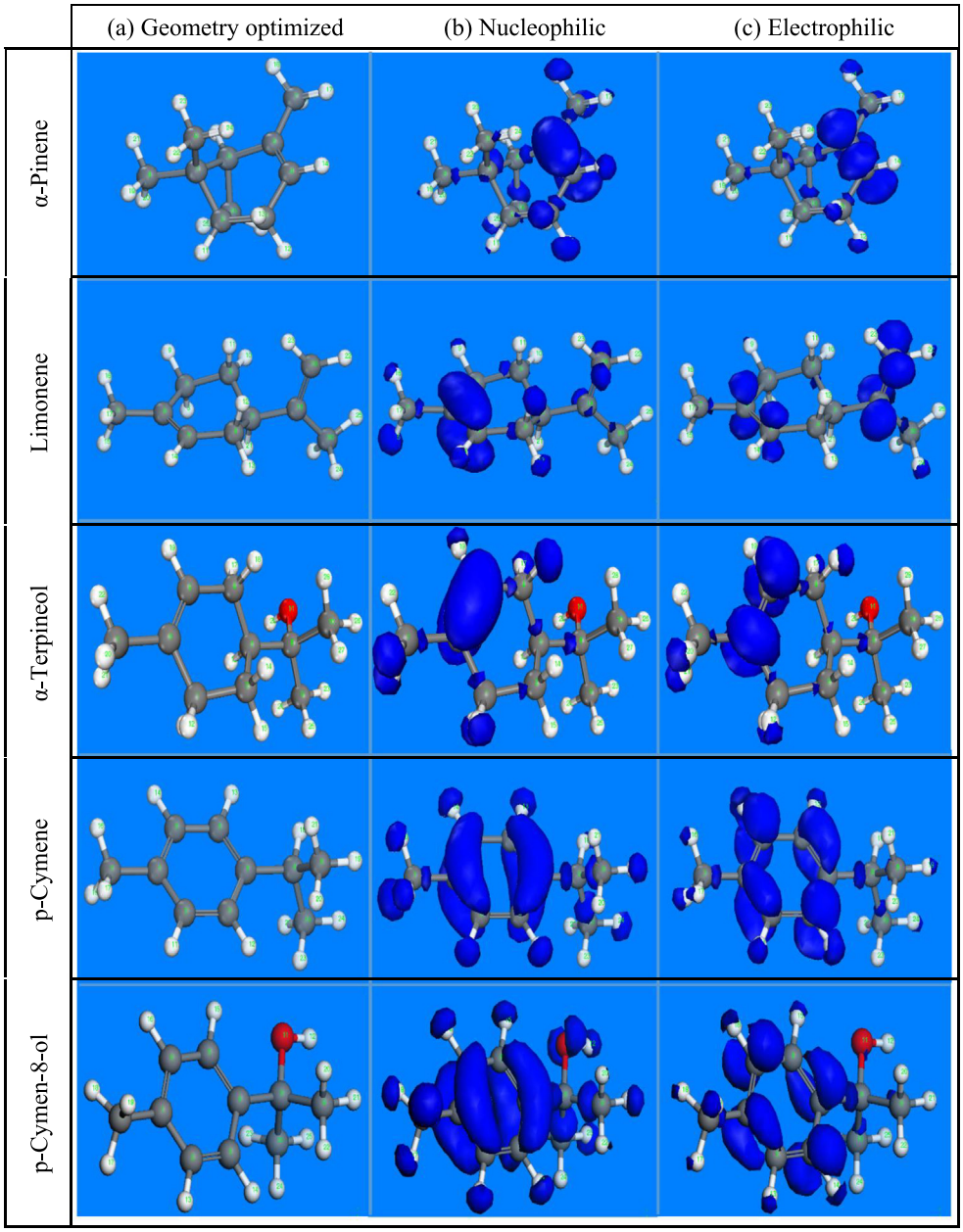

Fig. 5. Fukui functions for molecules calculated by DFT (Dmol3). (a) Geometry optimized structure, (b) Nucleophilic and (c) Electrophilic Fukui functions.

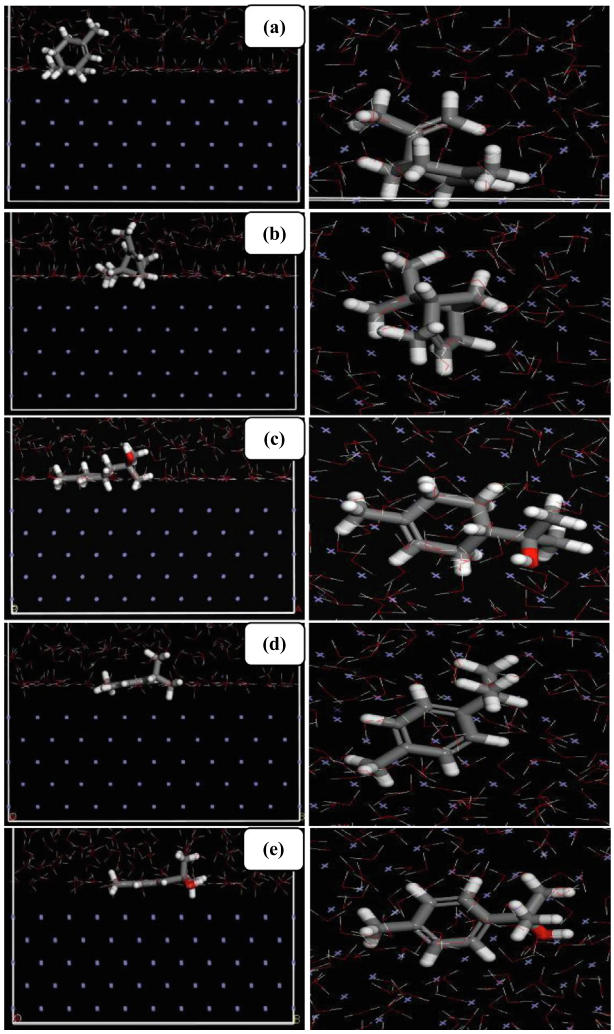

Fig. 6. Top and side views of the most stable low energy adsorption configurations of the inhibitors (a) Limonene, (b) α-Pinene, (c) α-Terpineol, (d) p-Cymene, (e) p-Cymen-8-ol, on Fe (1 1 0) surface using MD simulations.

Table 4
Interaction and binding energies obtained from MD simulations for adsorption of inhibitors on Fe (1 1 0) surface.

System	$E_{interaction}$ (KJ/mol)	$E_{binding}$ (KJ/mol)
Fe + α-Terpineol + 494 H_2O + $6Cl^-$ + $6Na^+$	−447	447
Fe + p-Cymen-8-ol + 494 H_2O + $6Cl^-$ + $6Na^+$	−446	446
Fe + p-Cymene + 494 H_2O + $6Cl^-$ + $6Na^+$	−385	385
Fe + Limonene + 494 H_2O + $6Cl^-$ + $6Na^+$	−312	312
Fe + α-Pinene + 494 H_2O + $6Cl^-$ + $6Na^+$	−282	282

tors donates electrons to the iron surface particularly α-Pinene inhibitor.

As shown in Table S5, it can be seen that for α-Terpineol and Limonene molecules high values of f_k^- are located on the C(2), C (5), C(1), and H(14), this reflects that the presence of double bond on cyclohexene of both compounds are responsible for electrons donating to the metal surface, on the other hand, C(10), H(3), and H(9) atoms are participating with electrons acceptance. In α-Pinene the values of negative fukui indices f_k^- indicate that C(4), H(14), H(5) are responsible for electrophile attacks, while C(5), C (12) and H(13) atoms with high values of f_k^+ indicate that these positive sites are able to accept electrons from metal surface. p-Cymen-8-ol and p-Cymene gives high negative fukui indices in C (4), C(5), C(6), C(7), H(22), H(23) and H(24) which indicate that benzene ring of these compounds has good electron-donating character. These results confirm the reactivity of these inhibitors with the iron surface.

As can be seen from Fig. 5, that the most reactive sites are C(4), C(5) for α-Pinene; C(5), C(6) for Limonene and α-Terpineol, while for p-cymene and p-cymen-8-ol inhibitors it appears that all carbon atoms of the ring are reactive.

- Molecular dynamics (MD) simulations results

The calculated of the interaction energies of the adsorbed inhibitors is made when the whole simulation system achieved its equilibrium state. The best favorable adsorption configuration of the studied molecules on Fe (1 1 0) surface is exposed in Fig. 6, as regards the interaction and binding energies are grouped in Table 4.

It must be emphasized that all five inhibitors adopt near-flat orientation on the surface of Fe (1 1 0). This way of adsorption can favor optimized interactions with the iron surface. In addition to that, the existence of the oxygen atoms, aromatic ring as well as conjugated double bonds in the molecular structure of our inhibitors, can facilitate donor-acceptor interactions, this allows the inhibitor molecules to prevent the iron surface from corrosion attack through a formation of a barrier layer between the iron surface and the aggressive media. The high negative energy suggests the strong and stable adsorption of the five inhibitors on Fe (1 1 0) surface (Xie et al., 2015; Zeng et al., 2011). The results are shown in Table 4 clarify that the binding energy of α-Terpineol is far higher than that of p-Cymen-8-ol, p-Cymene, Limonene and subsequently α-Pinene, hence, has less adsorption efficiency, which can be explained by the presence of the oxygen atom and π-electrons on α-Terpineol and p-Cymen-8-ol, while the lack of this oxygen in the three other inhibitors. These results are in good accordance with the experimentally obtained inhibition efficiency, which suggests that the Terebinth fruit EO is rich in α-Terpineol presents the high inhibition efficiency as compared to the EOs inhibitors of twigs and leaves of Terebinth. Based on the results of DFT and MD simulations, it can be concluded that the α-Terpineol acts as the major component, but the total inhibition action can be attributed to the intermolecular synergistic effect of various constituents of the Terebinth oils. This can be explained on the basis that the other molecular have a greater tendency to be absorbed on the surface.

4. Conclusion

The present work revealed that the Terebinth EOs acts as an effective, natural and environmentally friendly corrosion inhibitors for iron in neutral chloride medium at room temperature. Assessing the results of electrochemical measurements noted that the inhibition effects of the Terebinth EOs increased by increasing its concentrations. The Terebinth fruit EO showed maximum inhibition efficiency (86.4%) at the optimum concentration (3000 ppm). The results of potentiodynamic polarization curves indicated that the Terebinth EOs are mixed type inhibitors affecting both the anodic and the cathodic processes. Data obtained from theoretical DFT and MD simulations studies showed that the tested compounds of the corrosion inhibitors had good corrosion inhibition performance and exhibited high binding energies. Moreover, the theoretical outcomes indicated that the α-Terpineol (447 Kcal/mol) had the highest binding energy in comparison to the other tested compounds. This can be explained on the basis that the Terebinth fruit EO

which is rich in α-Terpineol has a maximum inhibition efficiency. This result indicates that both experimental and theoretical calculations are in reasonable agreement. SEM/EDX studies also strengthen all the findings. From the outcome of our study, it is possible to conclude that the essential oils of fruits, twigs and leaves from Terebinth can be applied as green corrosion inhibitors for iron corrosion in 3% NaCl solution.

Appendix A. Supplementary data

Supplementary data to this article can be found online at https://doi.org/10.1016/j.jksus.2020.08.004.

References

Adib Ghaleb, Aouidate, A., Lakhlifi, T., Bouachrine, M., Maghat, H., Sbai, A., 2018. Theoretical study of copper acetonitrile effects on parr functions indices and regioselectivity using Density Functional Theory (DFT). Russ. J. Phys. Chem. 92 (12), 2464–2471.

Alibakhshi, E., Ramezanzadeh, M., Haddadi, S.A., Bahlakeh, G., Ramezanzadeh, B., Mahdavian, M., 2019. Persian Liquorice extract as a highly efficient sustainable corrosion inhibitor for mild steel in sodium chloride solution. J. Clean. Prod. 210, 660–672.

Alparslan, Y., 2018. Antimicrobial and antioxidant capacity of biodegradable gelatin film forming solutions incorporated with different essential oils. Food Measure 12 (1), 317–322.

Alvarez, P.E., Fiori-Bimbi, M.V., Neske, A., Brandán, S.A., Gervasi, C.A., 2018. *Rollinia occidentalis* extract as green corrosion inhibitor for carbon steel in HCl solution. J. Indus. Eng. Chem. 58, 92–99.

Amar, H., Tounsi, A., Makayssi, A., Derja, A., Benzakour, J., Outzourhit, A., 2007. Corrosion inhibition of Armco iron by 2-mercaptobenzimidazole in sodium chloride 3% media. Corros. Sci. 49 (7), 2936–2945.

Aouniti, A., Azzouzi, M.E., Belfilali, I., Warad, I.K., Elmsellem, H., Hammouti, B., Jama, C., Bentiss, F., Zarrouk, A., 2018. Anticorrosion Potential of New Synthesized Naphtamide on Mild Steel in Hydrochloric Acid Solution: Gravimetric, Electrochemical, Surface Morphological, UV-Visible and Theoretical Investigations. Anal. Bioanal. Electrochem. 10, 1193–1210.

Asadi, N., Ramezanzadeh, M., Bahlakeh, G., Ramezanzadeh, B., 2019. Utilizing *Lemon Balm* extract as an effective green corrosion inhibitor for mild steel in 1M HCl solution: a detailed experimental, molecular dynamics, Monte Carlo and quantum mechanics study. J. Taiwan Inst. Chem. Eng. 95, 252–272.

Atarés, L., Chiralt, A., 2016. Essential oils as additives in biodegradable films and coatings for active food packaging. Trends Food Sci. Technol. 48, 51–62.

Bahlakeh, G., Ramezanzadeh, B., Dehghani, A., Ramezanzadeh, M., 2019. Novel cost-effective and high-performance green inhibitor based on aqueous *Peganum harmala* seed extract for mild steel corrosion in HCl solution: detailed experimental and electronic/atomic level computational explorations. J. Mol. Liq. 283, 174–195.

Barbouchi, M., Benzidia, B., Idrissi, M.E., 2019. Pistacia lentiscus L. Essential oils as a green corrosion inhibitors for iron in neutral chloride media. Anal. Bioanal. Electrochem. 11, 333–348.

Bentiss, F., Gassama, F., Barbry, D., Gengembre, L., Vezin, H., Lagrenée, M., Traisnel, M., 2006. Enhanced corrosion resistance of mild steel in molar hydrochloric acid solution by 1,4-bis(2-pyridyl)-5H-pyridazino[4,5-b]indole: electrochemical, theoretical and XPS studies. Appl. Surf. Sci. 252 (8), 2684–2691.

Benzidia, B., Hammouch, H., Dermaj, A., Benassaoui, H., Abbout, S., Hajjaji, N., 2019. Investigation of green corrosion inhibitor based on *Aloe vera* (L.) burm. F. for the protection of bronze B66 in 3% NaCl. Anal. Bioanal. Electrochem. 11, 165–177.

Bozorg, M., Shahrabi Farahani, T., Neshati, J., Chaghazardi, Z., Mohammadi Ziarani, G., 2014. *Myrtus Communis* as Green Inhibitor of Copper Corrosion in Sulfuric Acid. Ind. Eng. Chem. Res. 53 (11), 4295–4303.

Bozorgi, M., Memariani, Z., Mobli, M., Salehi Surmaghi, M.H., Shams-Ardekani, M.R., Rahimi, R., 2013. Five Pistacia species (P. vera , P. atlantica , P. terebinthus , P. khinjuk , and P. lentiscus): a review of their traditional uses, phytochemistry, and pharmacology. Sci. World J. 2013, 1–33.

Chugh, B., Singh, A.K., Chaouiki, A., Salghi, R., Thakur, S., Pani, B., 2020. A comprehensive study about anti-corrosion behaviour of pyrazine carbohydrazide: Gravimetric, electrochemical, surface and theoretical study. J. Mol. Liq. 299, 112160. https://doi.org/10.1016/j.molliq.2019.112160.

Dehghani, A., Bahlakeh, G., Ramezanzadeh, B., 2019. A detailed electrochemical/theoretical exploration of the aqueous *Chinese gooseberry* fruit shell extract as a green and cheap corrosion inhibitor for mild steel in acidic solution. J. Mol. Liq. 282, 366–384.

Domingo, L.R., Pérez, P., 2011. The nucleophilicity N index in organic chemistry. Org. Biomol. Chem. 9 (20), 7168. https://doi.org/10.1039/c1ob05856h.

Domingo, L.R., Ríos-Gutiérrez, M., Pérez, P., 2016. Applications of the conceptual density functional theory indices to organic chemistry reactivity. Molecules 21, 1-22.

El Aoufir, Y., Lgaz, H., Bourazmi, H., Kerroum, Y., Ramli, Y., Guenbour, A., Salghi, R., El-Hajjaji, F., Hammouti, B., Oudda, H., 2016. Quinoxaline derivatives as corrosion inhibitors of carbon steel in hydrochloridric acid media: electrochemical, DFT and monte carlo simulations studies. J. Mater. Environ. Sci. 7, 4330–4347.

Foddai, M., Kasabri, V., Afifi, F.U., Azara, E., Petretto, G.L., Pintore, G., 2015. In vitro inhibitory effects of Sardinian *Pistacia lentiscus* L. and Pistacia terebinthus L. on metabolic enzymes: pancreatic lipase, α-amylase, and α-glucosidase. Starch/Staerke 67, 204–212.

Haddadi, S.A., Alibakhshi, E., Bahlakeh, G., Ramezanzadeh, B., Mahdavian, M., 2019. A detailed atomic level computational and electrochemical exploration of the *Juglans regia* green fruit shell extract as a sustainable and highly efficient green corrosion inhibitor for mild steel in 3.5 wt% NaCl solution. J. Mol. Liq. 284, 682–699.

Hamadi, L., Mansouri, S., Oulmi, K., Kareche, A., 2018. The use of amino acids as corrosion inhibitors for metals: a review. Egypt. J. Pet. 27 (4), 1157–1165.

Jokar, M., Farahani, T.S., Ramezanzadeh, B., 2016. Electrochemical and surface characterizations of *morus alba pendula* leaves extract (MAPLE) as a green corrosion inhibitor for steel in 1M HCl. J. Taiwan Inst. Chem. Eng. 63, 436–452.

Kovačević, N., Kokalj, A., 2011. Analysis of molecular electronic structure of imidazole- and benzimidazole-based inhibitors: a simple recipe for qualitative estimation of chemical hardness. Corros. Sci. 53 (3), 909–921.

Macedo, R.G.M. de A., Marques, N.d.N., Tonholo, J., Balaban, R.d.C., 2019. Water-soluble carboxymethylchitosan used as corrosion inhibitor for carbon steel in saline medium. Carbohydr. Polym. 205, 371–376.

Majd, M.T., Asaldoust, S., Bahlakeh, G., Ramezanzadeh, B., Ramezanzadeh, M., 2019. Green method of carbon steel effective corrosion mitigation in 1 M HCl medium protected by Primula vulgaris flower aqueous extract via experimental, atomic-level MC/MD simulation and electronic-level DFT theoretical elucidation. J. Mol. Liq. 284, 658–674.

Mehta, Y., Trivedi, S., Chandra, K., Mishra, P.S., 2010. Effect of chromium on the corrosion behaviour of powder-processed Fe-0.45wt% P alloys. Sadhana 35 (4), 469–480.

Obot, I.B., Macdonald, D.D., Gasem, Z.M., 2015. Density functional theory (DFT) as a powerful tool for designing new organic corrosion inhibitors. Part 1: an overview. Corros. Sci. 99, 1–30.

Qiang, Y., Li, H., Lan, X., 2020. Self-assembling anchored film basing on two tetrazole derivatives for application to protect copper in sulfuric acid environment. J. Mater. Sci. Technol. 52, 63–71.

Qiang, Y., Zhang, S., Tan, B., Chen, S., 2018. Evaluation of *Ginkgo* leaf extract as an eco-friendly corrosion inhibitor of X70 steel in HCl solution. Corros. Sci. 133, 6–16.

Qiang, Y., Zhang, S., Zhao, H., Tan, B., Wang, L., 2019. Enhanced anticorrosion performance of copper by novel N-doped carbon dots. Corros. Sci. 161, 108193. https://doi.org/10.1016/j.corsci.2019.108193.

Rauf, A., Patel, S., Uddin, G., Siddiqui, B.S., Ahmad, B., Muhammad, N., Mabkhot, Y.N., Hadda, T.B., 2017. Phytochemical, ethnomedicinal uses and pharmacological profile of genus *Pistacia*. Biomed. Pharmacother. 86, 393–404.

Saha, S.K., Hens, A., RoyChowdhury, A., Lohar, A.K., Murmu, N.C., Banerjee, P., 2014. Molecular dynamics and density functional theory study on corrosion inhibitory action of three substituted pyrazine derivatives on steel surface. Can. Chem. Trans. 2, 489–503.

Sanaei, Z., Ramezanzadeh, M., Bahlakeh, G., Ramezanzadeh, B., 2019. Use of *Rosa canina* fruit extract as a green corrosion inhibitor for mild steel in 1 M HCl solution: a complementary experimental, molecular dynamics and quantum mechanics investigation. J. Ind. Eng. Chem. 69, 18–31.

Sun, H., 1998. COMPASS: an ab initio force-field optimized for condensed-phase applicationsoverview with details on alkane and benzene compounds. J. Phys. Chem. B. 102, 7338–7364.

Tan, B., Zhang, S., Qiang, Y., Li, W., Li, H., Feng, L.i., Guo, L., Xu, C., Chen, S., Zhang, G., 2020. Experimental and theoretical studies on the inhibition properties of three diphenyl disulfide derivatives on copper corrosion in acid medium. J. Mol. Liq. 298, 111975. https://doi.org/10.1016/j.molliq.2019.111975.

Umoren, S.A., Solomon, M.M., Obot, I.B., Suleiman, R.K., 2019. A critical review on the recent studies on plant biomaterials as corrosion inhibitors for industrial metals. J. Ind. Eng. Chem. 76, 91–115.

Verma, C., Ebenso, E.E., Bahadur, I., Quraishi, M.A., 2018. An overview on plant extracts as environmental sustainable and green corrosion inhibitors for metals and alloys in aggressive corrosive media. J. Mol. Liq. 266, 577–590.

Xie, S.-W., Liu, Z., Han, G.-C., Li, W., Liu, J., Chen, ZhenCheng, 2015. Molecular dynamics simulation of inhibition mechanism of 3,5-dibromo salicylaldehyde Schiff's base. Comput. Theor. Chem. 1063, 50–62.

Zeng, JianPing, Zhang, JianYing, Gong, XueDong, 2011. Molecular dynamics simulation of interaction between benzotriazoles and cuprous oxide crystal. Comput. Theor. Chem. 963 (1), 110–114.